DOI: 10.15480/882.9368

Eighth International Symposium on Marine Propulsors
smp'24, Berlin, Germany, March 2024

Scouring induced by a confined propeller jet nearby a vertical quay structure: scale model tests

Jesús Macías-Lezcano[1], Toni Llull[1,2], Jochen Aberle[1]

[1] Leichtweiß-Institute for Hydraulic Engineering and Water Resources, Division of Hydraulic Engineering and River Morphology, Technische Universität Braunschweig, Braunschweig, Germany

[2] Dept. of Nautical Science and Engineering, Maritime Engineering Laboratory, Universitat Politècnica de Catalunya, Barcelona, Spain

ABSTRACT

The turbulent jet generated by a ship propeller may cause damages to sediment beds due to its erosive potential. When local erosion or scour appears nearby harbour infrastructure like berthing quay walls, the risk of failure increases. To further develop approaches for the determination of the scour depth and geometry at quay walls as a function of time, scale-model experiments were carried out in a flume using different boundary conditions. The temporal development of the scour geometry was obtained by scanning the bed at predefined time-steps using an array of 16 ultrasonic sensors. These measurements were supplemented by additional measurements using a Vectrino Profiler and the Structure-from-Motion-Photogrammetry technique. The results from the tests show consistent relations between the measured maximum scour depth and the wall and bed clearance distances, respectively, as well as the rotational speed of the propeller. Contrary to the expectations according to published equations to estimate scour depths, the results obtained in this study show a direct linear dependency between the maximum scour depth and the wall clearance distances for all the tested boundary conditions. Moreover, the data also reveal a consistent functional relationship between the main scour hole dimensions and the eroded volume.

Keywords

Confined propeller wash, closed-type quay wall, sediment transport, propeller jet induced scour, scale model tests

1 INTRODUCTION

More than 80% of the global trade volume and about 70% of the trade value is carried by sea and, consequently, handled by ports (UNCTAD 2023) showing that maritime transport plays a significant role in the international trade and for the global economy. In the 1970s, the total volume carried by sea was approximately 2,600 million tons, while in 2019 it increased to 11,000 million tons. Because of the rapid growth of the seaborne transport, which is forecasted to increase annually at a rate of 2.1% until the end of the present decade (UNCTAD 2023), more powerful engines had to be and still will be developed.

At the same time, it is known that the jet stream from ship propellers has a strong effect on the bed of waterways and port structures in terms of erosion. The generated erosion depends on many boundary conditions such as the clearance distance between the propeller axis and the bed, the grain size distribution of the bed material, and the distance to infrastructures that act as a barrier and impede the unrestricted development of the induced propeller wash. Moreover, the propeller type and its speed of rotation as well as the vessel-type have also an influence on the scouring of the bed (Penna et al. 2018, Ferraro et al. 2021).

Since the end of last century, the propeller jet induced scouring problem has been investigated, mostly under laboratory conditions, due to the difficult and restricted controllable conditions faced in field tests (Spitzer et al. 2012a, b). To investigate this phenomenon in the simplest way, many studies (e.g., Hamill 1987, Tan & Yüksel 2018, Penna et al. 2019) focused on the scouring induced by an isolated propeller, thus neglecting the influence of other ship parts (e.g., propeller nozzle, rudders or the ship hull) or structures (piles, open and closed berthing quays) that have an effect on the development of the jet and therefore, the scour. Nonetheless, these studies highlighted various parameters that significantly affect the scour geometry such as the diameter of the propeller (D_p), its rotational speed (n_p), and the bed clearance distance (Z_b). Hamill et al. (1999) proposed Equation (1) to estimate the longitudinal distance between the propeller face and the location of the maximum equilibrium scour depth under unconfined conditions. This distance is defined as X_{mu} and calculated as follows:

$$X_{mu} = Fr_d^{0.94} G \tag{1}$$

where X_{mu} = distance between the propeller face and the asymptotic maximum scour depth under unconfined conditions (m), G = clearance distance between the propeller tip and the bed (m), and Fr_d = densimetric Froude number (-):

$$Fr_d = \frac{U_0}{\sqrt{\left(\frac{\rho_S - \rho_W}{\rho_W}\right) g d_{50}}} \quad (2)$$

where U_0 = efflux velocity (ms^{-1}), ρ_s = sediment density (kgm^{-3}), ρ_w = water density (kgm^{-3}), g = gravitational acceleration (ms^{-2}), and d_{50} = mean particle size (m).

In addition, several approaches (e.g., Hamill 1987, Qurrain 1994, Hong et al. 2013) have been developed to predict the temporal development of the maximum scour depth and the equilibrium scour depth. Other studies (Hashmi 1993, Qurrain 1994, Wei 2018, Llull 2021) examined the scouring action at different types of quay walls, such as open quays, parallel and perpendicular closed-type walls, and combined quay walls using single and twin-screw propellers. Hamill et al. (1999) proposed an equation to estimate the maximum scour depth in a confined scenario based on the maximum scour depth for the unconfined case:

$$\frac{\varepsilon_{m,c} - \varepsilon_{m,u}}{Z_b + \varepsilon_{m,u}} + 1 = 1.18\left(\frac{X_w}{X_{mu}}\right)^{-0.2} \quad (3)$$

where $\varepsilon_{m,c}$ = maximum asymptotic scour depth under confined conditions (m), $\varepsilon_{m,u}$ = maximum asymptotic scour depth under unconfined conditions (m), and X_w = wall clearance distance (m). Later, Yüksel et al. (2019) developed a model for predicting the maximum scour depth at the toe of a quay wall which does not require any specific information regarding the unconfined scour geometry:

$$\frac{\varepsilon_{m,c}}{D_p} = 0.512 Fr_d^{2.27}\left(\frac{G}{d_{50}}\right)^{-0.65}\left(\frac{X_w}{D_p}\right)^{-0.543} \quad (4)$$

The aim of this paper is to show the erosion caused by a model ship´s propeller and, in particular, the effect of a vertical quay structure parallel to the plane of the propeller on the scour geometry as a function of several tested boundary conditions.

The paper is structured as follows: first, the methodology is presented, including the experimental setup, the material, and the description of three different methods to detect and measure the changes in bed morphology. Section 3 presents preliminary results of the laboratory tests and includes a discussion of the influence of the individual boundary conditions together with the presentation of an empirically derived relationship between the main scour hole dimensions and the eroded volume. The main findings of this study are summarized in section 4.

2 METHODOLOGY

2.1 Experimental Setup

The experiments were carried out in two different experimental facilities in the hydraulic laboratory of the Leichtweiß-Institute for Hydraulic Engineering and Water Resources (LWI) at Technische Universität Braunschweig, Germany. Experiments with free propellers were performed in a 30 m long, 2 m wide and 0.8 m deep flume, that was used as a tank during the experiments presented in this work. The tests including a ship hull of the stern part of a GMS inland vessel, which is commonly found in the Rhine river (scale 1:16; see Geisenhainer and Aberle 2013 or Núñez-González et al. 2017 for details on the vessel) were carried out in a 14.5 m long, 5 m wide and 2 m deep reinforced concrete tank.

In the flume experiments, the bed slope was horizontal and a sediment recess (3 m in spanwise direction, 1 m in axial direction and 0.5 m deep) that modelled the mobile bed was placed against one of the acrylic walls of the flume, which acted as a closed-type quay wall and allowed visual monitoring and camera recording during the course of the experiment (Figure 1 right). In the case of the tank experiments, the sediment recess section measured 4.5 m in spanwise direction, 2 m in axial direction, and was 0.665 m deep. The quay structure was built from plywood plates that supported an acrylic wall, allowing also visual monitoring and camera recording (Figure 1 left). Both the flume and the tank were filled with water taken from the laboratory water system. All tests were carried out with still water conditions, i.e., without background flow. After the finalization of each test, the flume and tank, respectively, were carefully drained without disturbing the sand bed and the developed scour geometry.

The mobile bed consisted of different grain sizes in the experiments. Most of the tests were performed with coarse sand as bed material (CS; d_{50} = 0.0008 m and a coefficient of uniformity c_u = 1.74). Finer sediment, classified as medium sand (MS; d_{50} = 0.0002 m and c_u = 2.04), was also used as well as fine gravel (FG; d_{50} = 0.0041 m and c_u = 1.73). As c_u, computed as defined in Equation 5, is less than 5 for all bed types, their grain size distributions can be considered as uniform.

$$c_u = \frac{d_{60}}{d_{10}} \quad (5)$$

Figure 1. Experimental setup in the tank (left) and in the flume (right).

2.2 Propeller

Two propeller types with a diameter of D_p = 11 cm and a hub diameter of D_h = 2 cm were used in the experiments, a physical model of i) a Kaplan P274r propeller (Figure 2 left) and ii) a Wageningen B-Series 4-70 propeller (Figure 2 right) which had a geometrical scale of 1:16. The four-blade Kaplan P274r right-handed propeller had a pitch ratio of P/D_p = 1.1, an expanded blade area ratio EAR = 0.55, and a thrust coefficient of K_t = 0.49. The four-blade right-

handed Wageningen B4-70 propeller had a pitch ratio of P/D_p = 1.0, an expanded blade area ratio EAR = 0.7, and a thrust coefficient of K_t = 0.47.

The rotational movement of the propellers was achieved by means of a shaft connected to an electric motor which was equipped with an adjustable frequency drive (AFD). The linear relationship between the frequency set on the AFD and the rotational speed of the propellers was determined by measuring the corresponding propeller revolutions with a laser revolution counter at different frequencies set on the AFD. For most of the tests performed, the rotational speed was n_p = 22.32 Hz. However, tests were also carried out at lower propeller rotational speeds of n_p = 19.8 Hz, 9.9 Hz and 5.02 Hz.

The efflux velocity U_0 (ms^{-1}) was computed according to Equation 6 proposed by Fuehrer and Römisch (1977):

$$U_0 = \xi D_p n_p \sqrt{K_t} \quad (6)$$

and is presented in Table 1 for all experimental boundary conditions. For a non-ducted propeller, the coefficient ξ = 1.59, while for a ducted propeller, ξ = 1.12. The thrust coefficient K_t for each propeller was obtained from open water efficiency tests performed by the manufacturer.

Table 1. Studied boundary conditions and computed efflux velocities U_0 (ms^{-1}) for the tested speeds of rotation of the different propeller based on Equation (6).

Propeller	n_p (Hz)	U_0 (ms^{-1})	X_w/D_p (-)	Z_b/D_p (-)
Kaplan	22.32	2.732	2 – 6	0.94 – 1.5
Kaplan*	22.32	1.925	4 – 8	0.94 – 2.5
Kaplan	19.8	2.424	2 – 6	0.94 – 1.5
Wageningen	22.32	2.676	2 – 6	0.94 – 1.5
Wageningen	19.8	2.374	2 – 6	0.94 – 1.5
Wageningen	9.9	1.187	2 – 4	0.94
Wageningen	5.02	0.602	2 – 4	0.94

The tests series marked with * were performed with a stern ship hull, nozzle and double rudder. The corresponding efflux velocity was computed using Eq. (6) and ξ = 1.12.

Figure 2. Right-handed propellers used in the experiments; Left: Kaplan P274r propeller; Right: Wageningen B4-70 propeller. Both propeller have a propeller diameter of D_p = 0.11 m and an hub diameter of D_h = 0.02 m.

For the tests presented in this paper, no flow velocity measurement has been performed. However, flow velocity studies in another project using the same propellers have shown a good agreement between the measured efflux velocities and those estimated using Eq. (6) (Núñez-González et al. 2017, LWI 2019).

2.3 Experimental Program

In the experiments, X_w and Z_b, defined in Figure 3, were systematically changed. Overall, the boundary conditions of each experiment were defined by X_w, Z_b, U_0 and the use of a free propeller or ship-mounted propeller. In the following, the following abbreviations are used: S - with stern ship hull; DR - double rudder; and N - nozzle. It needs to be mentioned that, for these specific boundary conditions, only the Kaplan propeller was used.

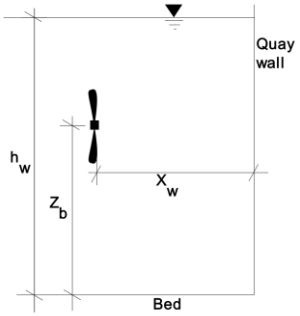

Figure 3. Definition of the boundary conditions X_w, Z_b and h_w.

2.4 Methods

Three different measurement techniques were used to measure the maximum scour depth. Regardless of the measuring technique employed, the flat bed was measured before the start of the experiment and defined the reference level. The scour depth measurements were obtained at pre-defined time intervals at which the experiments were stopped and then continued after the measurement. As stated by Hamill (1987), turning on and off of the propeller does not affect the overall scour geometry. In accordance with previous research performed at the LWI-laboratory, the propellers were turned off and the scour was measured at t = 10, 30, 70, 150, 310, 630, 1280, 2550, 5110, 7200 and 10230 s after the start of each test. The measurements at the different time steps were later subtracted from the reference level, so that the scour geometry could be referenced to the flat bed elevation which defined the origin of the vertical axis, i.e., z = 0. Thus, deposits are defined as positive bed elevation data while the negative bed elevation data define eroded zones.

The primary method employed to obtain the time-evolution of the bed morphology was the full scanning of the bed by a 5-MHz SeaTek Ultrasonic Ranging System (URS), arranged in an array of 16 sensors that could be moved with a traverse system, which allowed the controlled movement along the x, y and z axes. The URS was used and validated in previous studies (e.g., Friedrich et al. 2005, 2008). The distance between each ultrasonic sensor was 0.05 m, and a sampling rate of 10 Hz was used in conjunction with a translational speed of the traverse of 0.02 ms^{-1} resulting in a spatial resolution of 0.002 mm along each scour profile. The raw ultrasonic sensors data was post-processed and

fitted to a grid of 0.005 x 0.005 m to obtain the 3D surface of the sediment bed at each time-step.

At the end of each experiment, the 3D surface of the sediment bed was additionally obtained by means of the Structure-from-Motion Photogrammetry technique (SfM). Overlapping images of the bed surface were taken with a DSLR-Nikon D7200 camera with a Nikon DX VR, AF-S NIKKOR 18-140mm 1:3.5-5.6G ED camera lens and subsequently processed with the software *Agisoft Metashape Professional*. Approximately 100 photos were taken in dry conditions before starting each experiment to obtain the digital model of the flat bed and after completion of the experiment to obtain the digital model of the scour, as shown in Figure 4. The elevation error of the models, referenced to markers for their allocation and scaling, remained consistently below 0.0006 m.

Figure 4. Generated DEM using SfM-Photogrammetry.

In order to distinguish between the eroded and deposited volumes based on the SfM measurements, the bed elevation *z* was expressed as a function of x and y, i.e., z = f(x,y). Since the analytical solution of the scour volume is not known due to the discretization into a grid along the bed's domain, the eroded volume V_{erod} was calculated using the numerical integration according to:

$$V_{erod} = \iint_{xy} z(x,y)dxdy \approx$$

$$\approx \frac{\Delta x}{2}\sum_{j=1}^{m-1}\frac{\Delta y}{2}\sum_{i=1}^{n-1}(z_{i,j} - z_{i+1,j+1}) \qquad (7)$$

where m and n denote the number of discretization elements along the x- and y-axis, respectively.

Finally, a Vectrino Profiler was also used to measure the bed level along the transverse and longitudinal bed profiles containing the maximum depth without draining the flume and tank. The longitudinal profile was taken along propeller axis while the transverse profile was aligned parallel to the quay wall at the minimum possible distance (5 cm). The sampling rate was set to 10 Hz and the traverse speed was 0.015 m/s resulting in a spatial resolution along the corresponding profile of 0.0015 m. These profiles were acquired after each time step before continuing the experiment to determine the time evolution of both profiles. It should be emphasised that there is no consensus on the definition of the equilibrium state of propeller wash induced scour. In this paper, we consider that was reached when the temporal rate of erosion (mh^{-1}) was less than 5% of the propeller diameter D_p.

3 RESULTS AND DISCUSSION

This section provides preliminary results of our (still ongoing) tests and their discussion. In a first step, the reproducibility of the experiments was examined by repeating specific experiments with the Wageningen propeller using the same boundary conditions which are defined in the legend of Figure 5.

Figure 5a and b present the maximum scour depths and widths, respectively, at designated time intervals (c.f. section 2.4). The figures show a good agreement with a deviation of less than 10% which is a strong indicator that the experimental reproducibility is given.

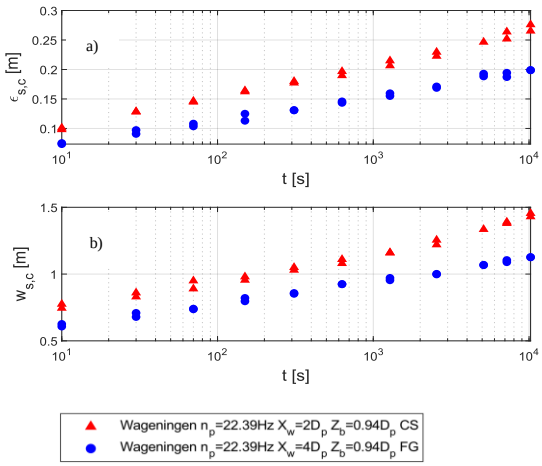

Figure 5. Maximum scour dimensions ((a) depth and (b) width) measured at different time-steps for identical boundary conditions.

3.1 Influence of Individual Boundary Conditions

3.1.1 Presence of a vertical quay structure

As stated in the introduction, the presence of a quay wall has a strong impact on the maximum scour depth. This can be clearly seen in Figure 6, which shows the temporal evolution of the maximum scour depth for the same boundary conditions as defined in the caption in Figure 6 except for the presence of a quay wall. For a direct comparison, the "no quay wall" case, which was studied in the framework of another project (Núñez-González et al. 2017, LWI 2019), is represented by empty markers in Figure 6. The filled markers represent the maximum scour depths for the "with quay wall" case, in which the propeller was placed at its closest distance from the quay wall ($2D_p$ and $4D_p$ for the cases "free propeller" and "ship-mounted propeller", respectively).

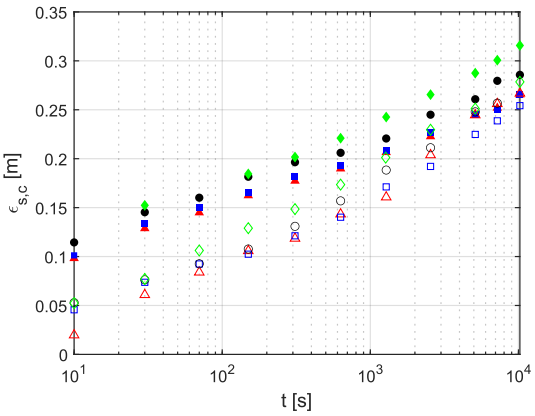

Figure 6. Comparison between maximum scour depth without a quay wall (empty markers) and with a quay wall

(filled markers). Triangle markers: Wageningen n_p = 22.39 Hz, X_w = 2 D_p, Z_b = 0.94 Dp, CS; Square markers: Wageningen n_p = 19.8 Hz, X_w = 2 D_p, Z_b = 0.94 D_p, CS; Circle markers: Kaplan n_p = 22.39 Hz, X_w = 2 D_p, Z_b = 0.94 D_p, CS; Diamond markers: Kaplan n_p =22.39 Hz, X_w = 4 D_p, Z_b = 0.94 D_p, CS, S, N, DR.

The figure clearly reveals the influence of the quay wall on the maximum scour depth, especially during the first time-steps.

3.1.2 Rotational speed n_p, bed clearance distance Z_b and particle size d_{50}

Both the scour depth and scour width increase with the propeller speed of rotation, as shown by Figure 7. Furthermore, the inverse relationship between the main scour dimensions and the bed clearance distance and bed grain size, respectively, were also confirmed in the results (see Figures 8 and 9). Similar trends have been already found by other researchers (e.g. Tan and Yüksel 2018, Yüksel et al. 2019, Penna et al. 2018 and Ferraro et al. 2021).

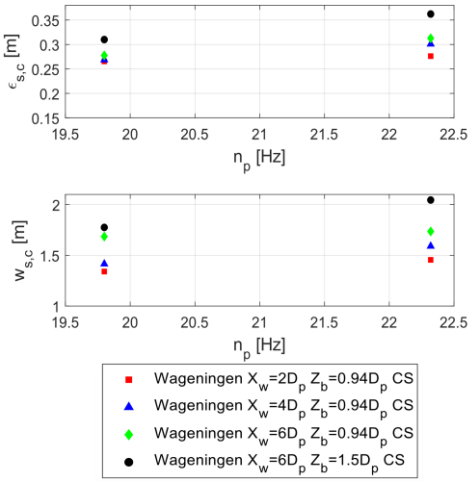

Figure 7. Maximum equilibrium scour depths and widths measured in dependency of n_p.

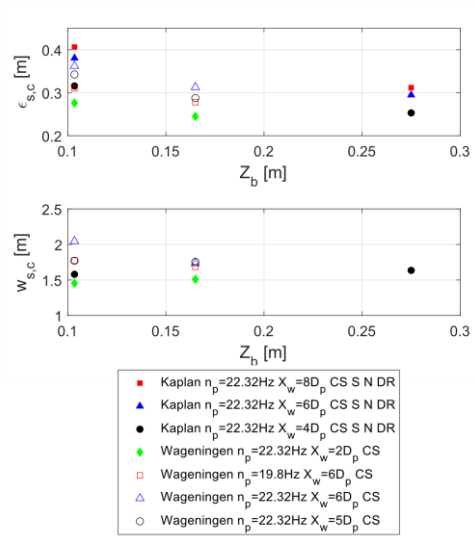

Figure 8. Maximum equilibrium scour depths and widths as a function of Z_b.

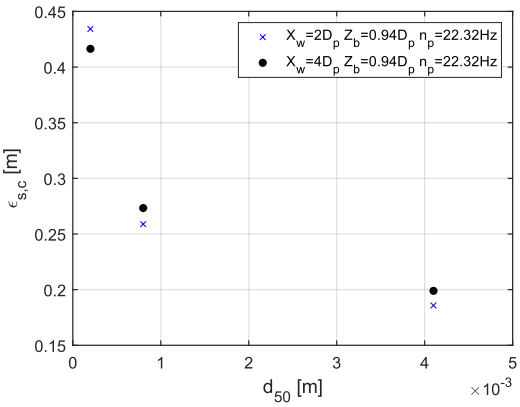

Figure 9. Maximum equilibrium scour depth as a function of d_{50} for experimental series with the Wageningen propeller.

3.1.3 Wall clearance distance X_w

The effect of the wall clearance distance X_w on the maximum scour depth is exemplarily shown in Figure 10 for a representative part of the test results. Contrary to expectations, a direct linear relationship between X_w and the maximum scour depth was identified for all conditions. This contradicts previous findings expecting an inversely proportional relationship between the primary scour hole dimensions and X_w, i.e., it would have been expected that a smaller wall clearance distance will result in a deeper and wider scour hole, which was not the case in the present experiments. On the other hand, the results support the conclusion of Wei (2018) that two different mechanisms exist for the formation of scour holes around open quays which depend on the longitudinal distance between the propeller face and the location of the maximum scour depth in the unconfined condition (X_{mu}, see Equation 1). In fact, our data indicate a direct linear relationship between the scour depth and the distance to the wall for $X_w < X_{mu}$. Note that, in cases where the wall is located further downstream of X_{mu}, an inverse relation between the wall clearance and the scour depth would be expected (Wei 2018).

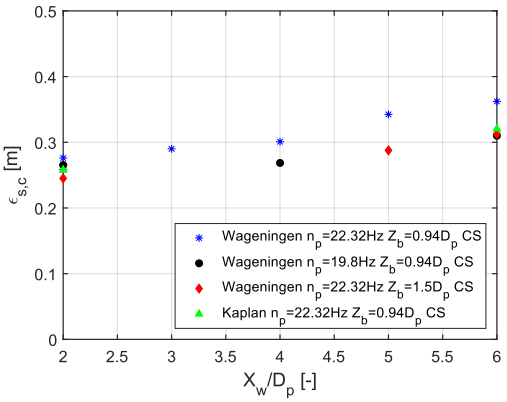

Figure 10. Relationship between the normalised wall clearance distance X_w/D_p and the maximum scour depth.

In our experiments, the wall clearance distances X_w were always smaller than X_{mu} which is the reason that a thorough analysis of the scour formation for this case has not yet been conducted. Nonetheless, it can be hypothesized that

the two mentioned different mechanisms also apply to scenarios involving closed-type quay walls.

3.2 Geometric Relationship of Induced Scour Holes

Curulli et al. (2022) analysed the relationship between the main scour hole dimensions and the eroded sediment volumes (V_{erod}) induced by a twin-propeller. A similar approach was adopted in this work for the case of single screw propellers. Curulli et al. (2022) found no relationship between the dimensionless eroded volumes (V_{erod}/X_w^3 or V_{erod}/Z_b^3) and the dimensionless scour widths ($w_{s,c}/X_w$ or $w_{s,c}/Z_b$). However, for the present experiments with single screw propellers, a relationship between the volume and width was identified regardless of the boundary conditions or the normalization variable (X_w or Z_b):

$$\frac{V_{erod}}{X_w^3} = 0.0094\left(\frac{w_{s,c}}{X_w}\right)^{3.304} \quad (8)$$

$$\frac{V_{erod}}{Z_b^3} = 0.0347\left(\frac{w_{s,c}}{Z_b}\right)^{2.675} \quad (9)$$

Both trends are presented in Figure 11 together with experimental data (R^2 = 0.9735 and 0.9535 for Equations (8) and (9), respectively). On the other hand, Curulli et al. (2022) found a relationship between the dimensionless eroded volume (V_{erod}/X_w^3 or V_{erod}/Z_b^3) and the dimensionless scour depth ($\varepsilon_{s,c}/X_w$ or $\varepsilon_{s,c}/Z_b$), which was also found in the present study (R^2 = 0.9865 and 0.9914, respectively):

$$\frac{V_{erod}}{X_w^3} = 2.6609\left(\frac{\varepsilon_{s,c}}{X_w}\right)^{2.8548} \quad (10)$$

$$\frac{V_{erod}}{Z_b^3} = 2.9399\left(\frac{\varepsilon_{s,c}}{Z_b}\right)^{2.868} \quad (11)$$

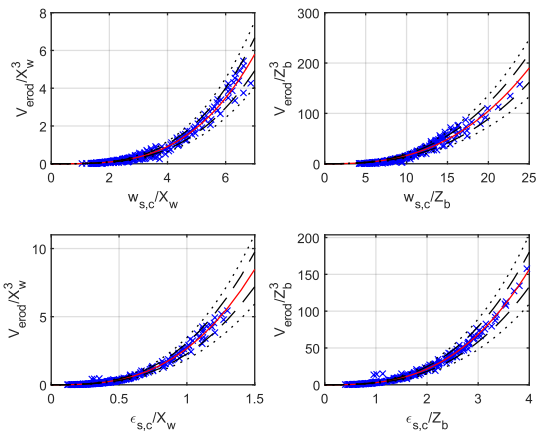

Figure 11. Relationship between the dimensionless eroded volume and dimensionless main scour dimensions by (left) X_w and (right) Z_b. Top figures: Main scour dimension is scour width $w_{s,c}$. Bottom figures: Main scour dimension is scour depth $\varepsilon_{s,c}$. The solid red line represents the perfect agreement of the models; while the dashed line, the ±15 % error limits, and the dots line, the ±30 % error bounds.

The similarity of Equations 8 – 11 indicates a near linear correlation between the scour width and depths, which is shown in Figure 12. We note that we observed increased scatter in data stemming from the experiments carried out with ship hull, rudder and nozzle, as these ship parts have a significant impact on the jet diffusion and, consequently, the induced scour (solid triangles in Figure 12). The linear model

$$w_{s,c} = 4.4699\varepsilon_{s,c} + 0.2848 \quad (12)$$

fits the dataset for the free propeller experiments (no ship hull, rudder or nozzle) with an R^2 of 0.9301 and a mean relative error of 7.15 %. Considering the data from all conducted experiments, the model is still valid, but the best new fit (with a reduced R^2 value of 0.7869 and an increased mean relative error of 10.74 %) is:

$$w_{s,c} = 4.638\varepsilon_{s,c} + 0.3019 \quad (13)$$

The effect of each ship component could not yet be fully analysed as no tests were conducted on adding solely one component. We note that propellers are not found with only one isolated component in real case scenarios, indicating the need for further investigations using also ship hulls. Such experiments are currently carried out in the LWI laboratory.

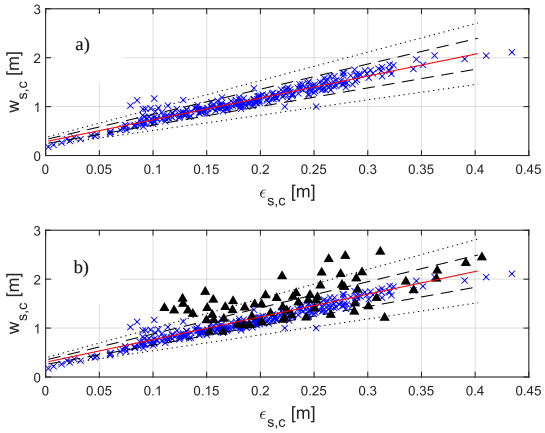

Figure 12. Relationship between scour depth and width for the set of boundary conditions (a) only with a free propeller and (b) the complete dataset. The solid red line represents the perfect agreement of the models; while the dashed line, the ±15 % error limits, and the dots line, the ±30 % error bounds.

3.3 Additional Scour Equation

Yüksel et al. (2019) proposed an equation for estimating the maximum scour depth at the toe of the quay wall, without considering the induced unconfined scour (see Equation 4). In contrast to Equation 4, we found direct proportional dependence between $\varepsilon_{s,c}/D_p$ and X_w/D_p showing that Equation 4 does not represent a suitable fit for our data. A comparison of the maximum scour depth and the calculated relative values is presented in Figure 13 in which only experiments within the range of validity, as

specified by Yüksel et al. (2019), are included ($7.73 \leq Fr_d \leq 15.01$ and $2.7 \leq X_w/D_p \leq 10.8$). The figure clearly shows the disagreement between the Yüksel et al. (2019) model and our experimental data.

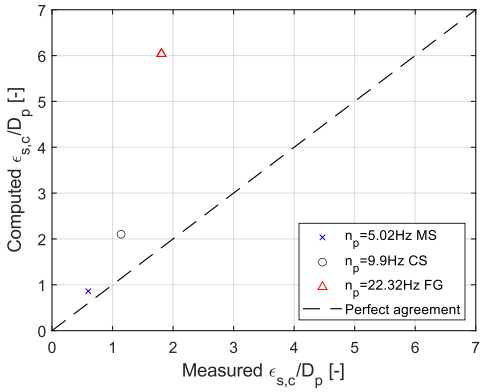

Figure 13. Comparison between the measured and computed maximum scour depths at the toe of the quay wall using Equation (4) by Yüksel et al. (2019). Boundary conditions: Wageningen propeller, $X_w = 4D_p$, $Z_b = 0.94\ D_p$.

Adjusting the factor and exponents of Yüksel et al. (2019) model (see Equation 4), we obtained a fit of the maximum scour depth at the toe of the quay wall, which simultaneously represented the maximum scour depth in its entirety for all tested conditions according to

$$\frac{\varepsilon_{m,c}}{D_p} = 0.162 Fr_d^{0.914} \left(\frac{G}{d_{50}}\right)^{-0.145} \left(\frac{X_w}{D_p}\right)^{0.278} \quad (14)$$

with R^2 = 0.852. Figure 14 illustrates the comparison between the measured and calculated dimensionless maximum scour depth at the quay wall for all the tested conditions, i.e., Fr_d, X_w/D_p. It is worth mentioning that no independent data have yet been used to validate the equation. We will follow this up in our further investigations.

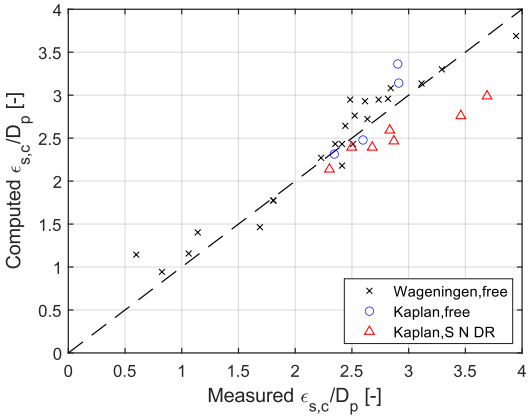

Figure 14. Comparison between the measured and computed maximum scour depth at the toe of the quay wall with Equation (14) for all the tested combinations of boundary conditions.

4 SUMMARY AND CONCLUSIONS

In this work, preliminary results of ongoing scouring tests performed with a vertical quay wall placed perpendicular to the propeller longitudinal axis, are presented. Various boundary conditions were systematically varied, such as the propeller rotational speed (n_p), the bed material (characterized by its median particle size d_{50}), and the distance to the bed (Z_b). The objective was to investigate the impact of each boundary condition on the maximum scour depth. As expected, a higher scour depth is found due to faster rotational speed n_p, reduced bed clearance distance and smaller grain size. We also identified the effect of the propeller type. As for cases with no quay wall, the induced scouring with a Kaplan propeller results in deeper scour holes than the Wageningen propeller. Contrary to expectations drawn from published equations for scour depths estimation, our findings indicate a direct proportional dependence between the maximum scour depth and the clearance distance from the wall for all the boundary conditions tested. It is suggested, that a direct proportionality between both parameters can only be observed if the quay wall is located between the propeller face and the position of the asymptotic maximum scour depth under unconfined conditions, X_{mu}, similarly to the scenarios tested by Wei (2018) with open quays.

The analysis of the scour hole geometry was based on the relationship between the eroded volume and the main dimensions of the scour hole, i.e., the maximum scour depth and width. The most accurate results were obtained by the description of the dimensionless eroded volume (V_{erod}/Z_b^3) dependent on the dimensionless maximum scour depth ($\varepsilon_{s,c}/Z_b$), with an R^2 value of 0.9914 and a mean relative error of 9.5 %. Moreover, a clear correlation between the scour width and the eroded volume was found, as well as between the scour width and depth. It should be noted that in cases where other ship parts (such as the ship hull, nozzle or rudders) are present, a larger data scatter was observed leading to an increased estimation error of the derived equations compared to the free propeller conditions.

Based on Yüksel et al. (2019) approach, an empirical equation has been suggested for scenarios where $X_w \leq X_{mu}$. The validity of the proposed equations should be considered only within the ranges of boundary conditions tested in this experimental series ($10.4 \leq Fr_d \leq 46.1$; $2.0 \leq X_w/D_p \leq 8.0$; $0.94 \leq Z_b/D_p \leq 2.5$). For generalization of the proposed formulas, additional experiments are needed.

ACKNOWLEDGMENTS

The authors thank Mrs. Lina Schulz and Mr. Florian Haselow, who took part in the experimental activity during their BSc theses and Mrs. Lisa Holste, who took part in the experimental activity during her MSc thesis. This research was carried out within the framework of the project "IHATEC – Innovative Hafentechnologien. Propellerstrahlinduzierte Erosionserscheinungen" funded by the german *Bundesministerium für Digitales und Verkehr*.

REFERENCES

Blaauw, H. G., van den Kaa, E. J. (1978). Erosion of bottom and sloping banks caused by the screw race of manoeuvring ships. 7th International Harbour Congress, Antwerp, Belgium.

Ferraro, D., Lauria, A., Penna, N., Gaudio, R. (2021). Temporal development of unconfined propeller scour in waterways. Phys. Fluids 33, 095119.

Friedrich, H., Melville, B. W., Coleman, S. E., Nikora, V. I., Clunie, T. M. (2005). Three-Dimensional measurement of laboratory submerged bed forms using moving probes. XXXI International Association of Hydraulic Engineering and Research Congress, Seoul, Korea, 96-404.

Friedrich, H., Melville, B.W. (2008). Topographical changes during bedform development. 8th International Conference on Hydro-Science and Engineering, Nagoya, Japan.

Fuehrer, M., Römisch, K. (1977). Effects of modern ship traffic on inland and ocean waterways and their structures. 24th International Navigation Congress, Leningrad, USSR.

Geisenhainer, P., Aberle, J. (2013). Scale model study of propeller induced scour development. In GeoPlanet: Earth and Planetary Sciences Series, doi:10.1007/978-3-642-30209-1_7.

Hamill, G. A. (1987). Characteristics of the screw wash of a manoeuvring ship and the resulting bed scour. Ph.D. thesis, Queen's University of Belfast, Northern Ireland, UK.

Hamill, G. A., Johnston, H. T., Stewart, D. P. (1999). Propeller wash scour near quay walls. Waterway, Port, Coastal, and Ocean Eng. 125:170-175.

Hashmi, H. N. (1993). Erosion of a granular bed at a quay wall by a ship's screw wash. Ph.D. thesis, Queen's University of Belfast, Northern Ireland, UK.

Hong, J. H., Chiew, Y. M., Cheng, N. S. (2013). Scour Caused by a Propeller Jet. Hydraulic Eng. 139:1003-1012.

Llull, T. (2021). Ship propeller induced scour of non-cohesive sediment in low bed-clearance conditions. Ph.D. thesis, Universitat Politècnica de Catalunya, Spain.

LWI (2019). Scour induced by inland ship propellers. Report No. 1098 (unpublished).

Núñez-González, F., Koll, K., Söhngen, B., & Spitzer, D. (2017). Scour geometry and flow velocities induced by an experimental ship propeller jet. 13th International Symposium on River Sedimentation, Stuttgart, Germany.

Penna, N., Alessandro, F. D., Gaudio, R., Tomasicchio, G. R. (2019). Three-dimensional analysis of local scouring induced by a rotating ship propeller. Ocean Eng. 188, 106294.

Qurrain, R. M. M. (1994). Influence of the sea bed and berth geometry on the hydrodynamics of the wash from ship´s propeller. Ph.D. thesis, Queen's University of Belfast, Northern Ireland, UK.

Spitzer, D., Söhngen, B., Aberle, J., Geisenhainer, P. (2012a). Belastung der Gewässersohle durch Propellerstrahlen - Teil 1: Untersuchungen bis zum Zweiten Weltkrieg. Korrespondenz Wasserwirtschaft, 5(4), 202-209.

Spitzer, D., Söhngen, B., Aberle, J., Geisenhainer, P. (2012b). Belastung der Gewässersohle durch Propellerstrahlen - Teil 2: Untersuchungen nach dem Zweiten Weltkrieg. Korrespondenz Wasserwirtschaft, 5(6), 321-330.

Tan, R. I., Yüksel, Y. (2018). Seabed scour induced by a propeller jet, Ocean Eng. 160, 132.

UNCTAD (2023). Review of maritime Transport 2023. United Nations Conference on Trade and Development, United Nations.

Verhey, H. (1983). The stability of bottom and banks subjected to the velocities in the propeller jet behind ships. 8th International Harbour Congress, Antwerp, Belgium.

Wei, M. (2018). Propeller jet flow and its associated scour hole around open quay structures. Ph.D. thesis, Nanyang Technological University, Singapore.

Yüksel, Y., Tan, R. I., Celikoglu, Y. (2019). Determining propeller scour near a quay wall. Ocean Eng. 188:106331.